*Journal of Applied Electrochemistry* **29**: 951–960, 1999.



# High energy ball-milled Pt and Pt–Ru catalysts for polymer electrolyte fuel cells and their tolerance to CO

M.C. DENIS[1], G. LALANDE[1]**, D. GUAY[1], J.P. DODELET[1]* and R. SCHULZ[2]
[1]*INRS-Énergie et Matériaux, C. P. 1020, Varennes, Québec, Canada, J3X 1S2;*
[2]*IREQ, Hydro-Québec, C. P. 1000, Varennes, Québec, Canada, J3X 1S1*
*(*author for correspondence)*
*(**Present address: IREQ, Hydro-Québec, C.P. 1000, Varennes, Québec, Canada, J3X 1S1)*

Received 24 July 1998; accepted in revised form 8 December 1998

*Key words:* anode, nanocrystalline, PEFC, PEM fuel cell, Pt–Ru alloy

**Abstract**

High energy ball milling, an industrially amenable technique, has been used to produce CO tolerant unsupported Pt–Ru based catalysts for the oxidation of hydrogen in polymer electrolyte fuel cells. Nanocrystalline $Pt_{0.5}$–$Ru_{0.5}$ alloys are easily obtained by ball-milling but their performances as anode catalysts are poor because nanocrystals composing the material aggregate during milling into larger particles. The result is a low specific area material. Improved specific areas were obtained by milling together Pt, Ru and a metal leacheable after the milling step. The best results were obtained by milling Pt, Ru, and Al in a 1:1:8 atomic ratio. After leaching Al, this catalyst ($Pt_{0.5}$–$Ru_{0.5}$ ($Al_4$)) displays a specific area of 38 $m^2\ g^{-1}$. $Pt_{0.5}$–$Ru_{0.5}$ ($Al_4$) is a composite catalyst. It consists of two components: (i) small crystallites (~4 nm) of a Pt–Al solid solution (1–3 Al wt %) of low Ru content, and (ii) larger Ru crystallites. It shows hydrogen oxidation performance and CO tolerance equivalent to those of $Pt_{0.5}$–$Ru_{0.5}$ Black from Johnson Matthey, the commercial catalyst which was found to be the most CO tolerant one in this study.

## 1. Introduction

Polymer electrolyte fuel cells (PEFCs) are highly efficient and low polluting electrical generators. Their use is contemplated in transportation and also in stationary applications [1–4]. PEFCs operate typically at 80–100 °C on $H_2$ mostly obtained by steam reforming methanol or other light hydrocarbon fuels (thermal decomposition, partial oxidation or autothermal reforming are also used [5]). PEFCs are not able to tolerate a CO level of about 1% by volume obtained, for instance, at the output of a methanol reformer. By using a shift process and a subsequent catalytic oxidizer, the CO level can be decreased to 1–100 ppm depending on the operating conditions of the oxidizer [6].

CO concentration in the hundred ppm range have a strong effect on the performances of PEFCs [7, 8]. Poisoning occurs because CO binds strongly to Pt sites resulting in a high Pt surface coverage of CO at the operating temperature of PEFCs. A first solution to this problem is to increase the temperature, but the operating temperature is limited to a maximum of about 120 °C by the need for effective humidification of the membrane [4]. A second solution consists of injecting a small amount of $O_2$ (up to about 2%) to oxidize CO chemically [7, 9, 10]. However, the explosion threshold for $H_2/O_2$ mixtures is 5% $O_2$ in $H_2$. This limits to about 100 ppm the maximum level of CO that can be treated effectively by oxygen bleeding in PEFCs [4]. Furthermore, the chemical oxidation of CO by $O_2$ catalysed by Pt at the anode reduces the amount of Pt available for producing a current from the oxidation of hydrogen. A third solution to the poisoning problem is to use Pt alloy catalysts that are more tolerant towards CO poisoning than pure Pt.

Among all binary alloys that have been considered for CO tolerance, Pt–Ru alloys are certainly those that have been the most studied. The use of Pt–Ru as oxidation catalyst for $H_2$ containing CO at the anode leads to a lowering of the CO oxidation potential (onset of CO oxidation at ~0.4 V vs RHE in 0.5 M $H_2SO_4$ [11]) compared with the oxidation potential of CO on pure Pt (onset of CO oxidation at ~0.7 V vs RHE in 0.5 M

$H_2SO_4$ [11]). CO poisoning is therefore alleviated [12, 13]. The activity of Pt–Ru alloys towards CO oxidation is related to their bifunctional properties [11, 14–16]: a nucleation at low potentials of oxygen containing species ($OH_{ads}$) on Ru atoms and the bimolecular reaction of $OH_{ads}$ with CO adsorbed on Pt. The optimum Pt–Ru surface composition for CO oxidation is $Pt_{0.5}$–$Ru_{0.5}$. Unsupported catalysts characterized by a Pt/Ru atomic ratio of 1 are available commercially. They are $PtRuO_x$ from E-TEK and Pt–Ru Black from Johnson Matthey. They have been used as catalysts in $H_2/O_2$ fuel cells and in direct methanol fuel cells [17, 18] for which CO poisoning at the anode is also of importance [19].

The aim of this work is to demonstrate that high energy ball milling (BM), a technique which is industrially amenable, may be considered as an interesting alternative technique to produce unsupported catalysts for fuel cells. It is known that by using the BM technique, it is possible to form a large number of alloys by direct reaction in the solid state between elemental components which are subject to intense mechanical deformation [20]. BM produces nanocrystalline or even amorphous metal alloys having properties quite different from conventional bulk alloys [21–24]. BM is obtained by the rapid movement of a hermetically sealed crucible containing the metal powders to be alloyed and several balls with which they enter into collision. The macroscopic temperature of the container and its contents barely increases a few tens of degrees during the process and it seems that the microscopic or local temperature does not increase more than 300 °C [25]. Alloys are then produced by the diffusion of the elements in the solid state which is favored by the appearance of defects in the crystalline structure after mechanical deformation.

As a first step towards demonstrating that BM is an interesting alternative technique for the production of fuel cell catalysts, it will be shown that CO tolerant Pt–Ru catalysts are obtained by BM with performances at least equivalent to commercial catalysts with an equivalent Pt/Ru ratio. This paper will also establish that a critical point in the use of the BM technique is to find methods to increase the specific area of the ball-milled nanocrystalline materials over the typical value of 1 $m^2\ g^{-1}$ usually obtained for powders prepared with this method.

## 2. Experimental details

### 2.1. *Catalyst preparation and characterization*

The various metal powders used in catalyst preparation were: Pt, $<74\ \mu m$ ($-200$ mesh) in size, 99.8% (Alfa AESAR); Ru, $<44\ \mu m$ ($-325$ mesh), 99.95% (Omega); Al, 44–420 $\mu m$ ($-40+325$ mesh) (Johnson Matthey Electronics); Mg, $<44\ \mu m$ ($-325$ mesh), 99.8% (Alfa Aesar). The catalysts were prepared using a Spex 8000 mixer/mill. Metal powders and WC balls were loaded in a 70 ml WC crucible. Unless otherwise specified, six grams of powder were used, and the ball-to-powder weight ratio was always 4/1. All powder handling was performed in an Ar-filled glove box, and the crucible was hermetically sealed with a Viton O-ring. Milling times of 40 h were routinely used. Between two metal millings, crucible and balls were cleaned by three consecutive 1 min runs with water to remove the remaining powder sticking on the crucible walls and on the balls.

The ball-milled materials were characterized by (i) X-ray diffraction (XRD) using a Siemens D-500 diffractometer equipped with a Cu$K_\alpha$ radiation source; (ii) surface area measurements by $N_2$ adsorption (multipoint BET) using a Quantachrome Autosorb automated gas sorption system; (iii) neutron activation analysis to obtain bulk concentrations of metals milled; and (iv) XPS using a VG Escalab 220i-XL equipped with an Al$K_\alpha$ monochromatic source.

### 2.2. *Electrochemical measurements*

The electrocatalytic performances of the catalysts were evaluated for pure $H_2$ (UHP, Praxair) and $H_2$ + 100 ppm CO (UHP, BOC Canada) in a GT60 GlobeTech fuel cell test station. The ink was prepared by sonicating for 20 min 40 mg of metal powder, 150 $\mu$l of a Nafion® 5 w/o solution (Aldrich), 400 $\mu$l of methanol (J. T. Baker, Cmos Electronic Grade), and 60 $\mu$l of glycerine (Fisher Scientific, ACS). A volume of 305 $\mu$l of the ink was pipetted onto a 5 $cm^2$ uncatalysed ELAT backing layer from E-TEK which was then dried in a vacuum oven for 1 h at 75 °C. The resulting catalyst loading was 4 mg $cm^{-2}$ a catalyst/Nafion® weight ratio of 85/15. A Pt catalysed ELAT backing layer (E-TEK, 0.37 mg Pt $cm^{-2}$) painted with a 5 w/o Nafion® solution was used as the cathode. After drying in a vacuum oven at 75 °C, the Nafion® deposited on the cathode amounted to 0.6 mg $cm^{-2}$.

Nafion 117® was used as the polymer electrolyte in the membrane electrode assembly. The membranes were cleaned by immersing them in boiling 3% $H_2O_2$(Fisher Scientific, ACS) for 1 h. Then, they were rinsed with deionized water and immersed for 1 h in boiling 0.5 M $H_2SO_4$ (Fisher Scientific, ACS) followed by 1 h in boiling deionized water. The membrane electrode assembly was obtained by hot-pressing the Nafion 117® membrane between the anode and the cathode at 140 °C for 40 s under 2500 psi. Current stabilization at 0.5 V

was reached before recording the polarization curves. These were obtained under the following conditions: cell temperature at 80 °C; temperature of water humidifying the anode and cathode gases at 110 °C; $H_2$ (or $H_2$ + 100 ppm CO) pressure at 30 psig; $O_2$(UHP, Praxair) pressure at 60 psig. $H_2$ and $O_2$ flow rates at 0.2 slm. For experiments involving CO, $H_2$ + 100 ppm CO was fed into the cell for 30 min under open circuit potential conditions before measuring the polarization curve.

Three commercial catalysts were used as references for the fuel cell tests. They were: platinum black (fuel cell grade, Alfa AESAR, Johnson Matthey) [Pt Black]; platinum ruthenium black (Pt 66%, Ru 34% (w/w), Alfa AESAR, Johnson Mattey) [$Pt_{0.5}$–$Ru_{0.5}$ Black]; and $PtRuO_x$ (Pt/Ru = 1/1 at, E-TEK) [$PtRuO_x$].

## 3. Results and discussion

### 3.1. *$Pt_{0.5}$–$Ru_{0.5}$ ball-milled catalysts*

Pt and Ru powders in a 1:1 atomic ratio were milled together to obtain $Pt_{0.5}$–$Ru_{0.5}$ nanocrystalline alloy. Figure 1 demonstrates that the alloy is obtained after 20 h of milling. The only phase detected by XRD, besides the WC contribution arising from crucible and ball attrition, is the f.c.c Pt structure. This structure is expected from the Pt + Ru phase diagram [26]. As the milling time increases from 0 to 20 h, the peaks associated with h.c.p Ru disappear while the Pt peaks shift to higher diffraction angles. This shift indicates a decrease in the dimensions of the unit cell caused by the substitution of Pt atoms in the lattice by smaller Ru atoms. All $Pt_{0.5}$–$Ru_{0.5}$ alloys used in fuel cell experiments have been milled during 40 h. They are labelled $Pt_{0.5}$–$Ru_{0.5}$ (BM).

Figure 2 presents the XRD diagrams of Pt Black (curve (a)) and $Pt_{0.5}$–$Ru_{0.5}$ (BM) (curve (b)). The diffractograms display wide peaks indicating the nanocrystallinity of both materials. The size of the nanocrystallites has been evaluated from the width at half height of the main diffraction peak (Pt(1 1 1)) corrected for the peak broadening due to the instrument [27]. Averages of 14 nm and 6 nm have been found for $Pt_{0.5}$–$Ru_{0.5}$ (BM) and Pt Black, respectively.

Figure 3 presents the $H_2/O_2$ polarization curve obtained at 80 °C for $Pt_{0.5}$–$Ru_{0.5}$ (BM) (dark triangles). This polarization curve is compared with polarization curves obtained in the same conditions (pure $H_2$) for the three reference catalysts (open symbols). Even if $Pt_{0.5}$–$Ru_{0.5}$ (BM) is a nanocrystalline material, its performance as a catalyst is very poor compared to those of

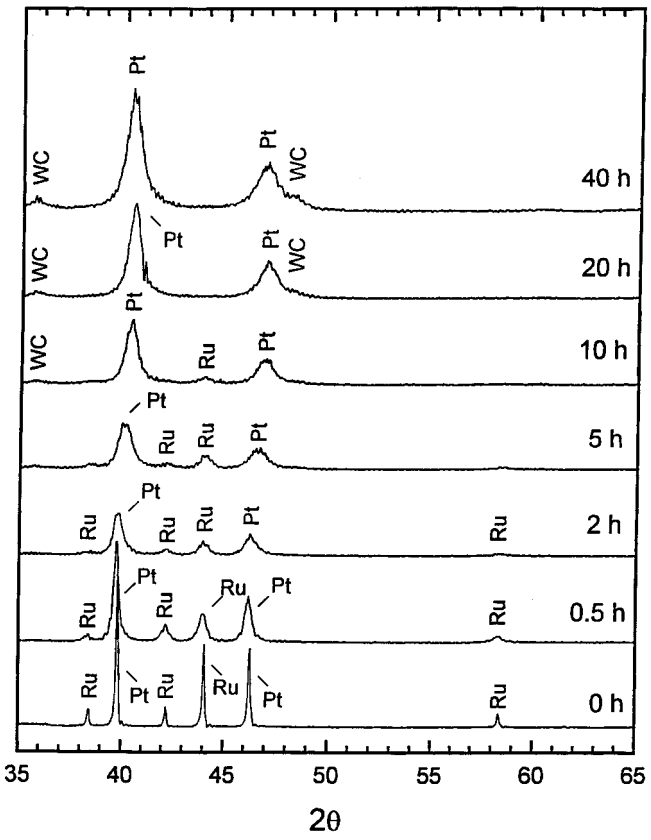


*Fig. 1.* X-ray diffractograms of a Pt : Ru mixture as a function of the milling time. The $Pt_{0.5}$–$Ru_{0.5}$ alloy phase is observed after 20 h of milling time.

commercial catalysts. BET measurements indicate that the specific area of $Pt_{0.5}$–$Ru_{0.5}$ (BM) is only 0.45 $m^2\ g^{-1}$ compared with 44.3, 145 and 63.2 $m^2\ g^{-1}$ for Pt Black, $PtRuO_x$, and $Pt_{0.5}$–$Ru_{0.5}$ Black, respectively. The low specific area is confirmed by SEM observations; nanocrystallite aggregates of micrometric dimensions are indeed observed in $Pt_{0.5}$–$Ru_{0.5}$ (BM). The poor performance of $Pt_{0.5}$–$Ru_{0.5}$ (BM) as an anode catalyst in fuel cells are therefore the result of the low specific area of that ball-milled material.

### 3.2. *$Pt_{0.5}$–$Ru_{0.5}$ (BM)–Mg ball-milled catalysts*

A dispersion technique was used to improve the specific area of $Pt_{0.5}$–$Ru_{0.5}$ (BM). This is based on a second milling of $Pt_{0.5}$–$Ru_{0.5}$ (BM) for 20 h with a dispersing metal like Al or Mg. The latter metal, which is readily oxidizable is leached in a subsequent step. A similar procedure was also used to increase the specific area of some nanocrystalline Mg obtained by ball-milling and used for hydrogen storage. In that case, the leached metal was Li [28].

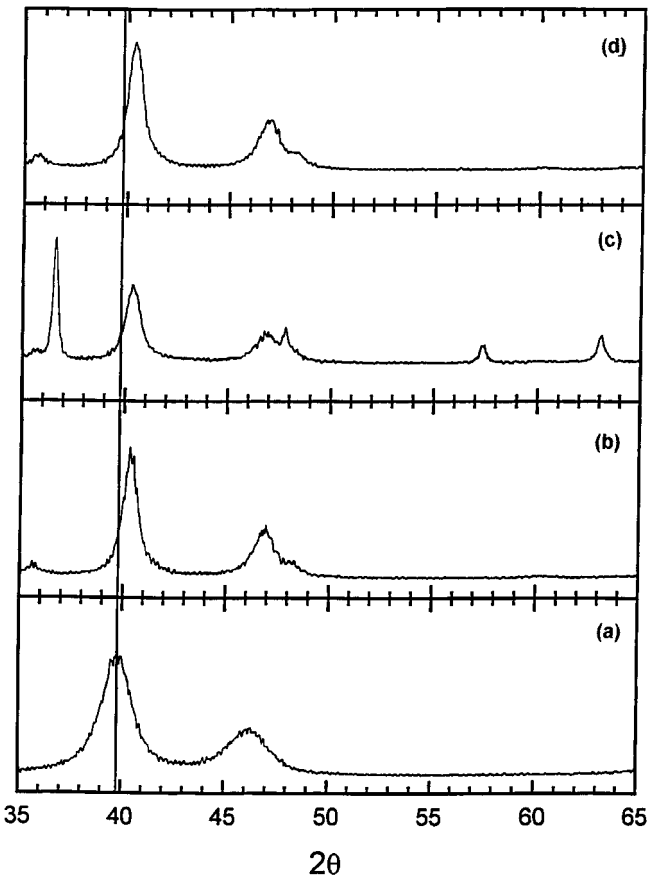


*Fig. 2.* X-ray diffractograms of: (a) Pt-Black, (b) $Pt_{0.5}$–$Ru_{0.5}$ (BM), (c) $Pt_{0.5}$–$Ru_{0.5}$ (BM) + Mg, (d) $Pt_{0.5}$–$Ru_{0.5}$ (BM)–Mg. Vertical line indicates the diffraction position of unalloyed Pt(1 1 1).

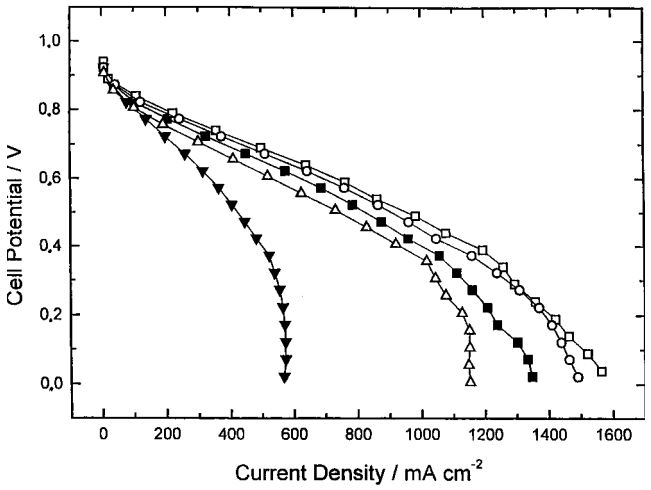


*Fig. 3.* $H_2/O_2$ polarization curves at 80 °C for a single membrane electrode assembly using (▼) $Pt_{0.5}$–$Ru_{0.5}$ (BM) and (■) $Pt_{0.5}$–$Ru_{0.5}$ (BM)–Mg at the anode. Polarization curves with (□) Pt Black, (○) $Pt_{0.5}$–$Ru_{0.5}$ Black and (△) $PtRuO_x$ at the anode are given for comparison.

Experimentally, 2 g of $Pt_{0.5}$–$Ru_{0.5}$ (BM) and 3 g of Al or Mg powder were introduced into a WC crucible with three WC balls. The dispersion attempt with Al was unsuccessful because the entire powder content stuck as a layer on the crucible walls and balls; it was impossible to remove this layer mechanically without damaging the crucible and the balls. On the other hand, the dispersion attempt with Mg was successful. The end product was then set in suspension by magnetic stirring for 8 h in a 1 M HCl solution. Mg was leached to yield a final powder which was filtered with deionized water and dried in a vacuum oven at 80 °C for 5 h before being used as anode catalyst.

By comparing in Figure 2 the diffraction spectrum of $Pt_{0.5}$–$Ru_{0.5}$ (BM) (curve (b)) with that of $Pt_{0.5}$–$Ru_{0.5}$ (BM) + Mg (curve (c)), which is the end product after a second milling, a superposition of sharp Mg peaks is seen on the diffractogram of $Pt_{0.5}$–$Ru_{0.5}$ (BM). Therefore, it may be concluded that Mg acts only as a dispersing agent, since there is no sign of Pt–Mg compounds in the X-ray spectrum. The dispersing character of Mg is also confirmed by the diffraction spectrum of $Pt_{0.5}$–$Ru_{0.5}$ (BM)–Mg (curve (d)) which is the final product obtained after leaching Mg from $Pt_{0.5}$–$Ru_{0.5}$ (BM) + Mg. Curve (d) has the same shape as curve (b). It shows that all Mg present as a dispersing agent has been removed from $Pt_{0.5}$–$Ru_{0.5}$ (BM) + Mg.

Figure 3 presents the $H_2/O_2$ polarization curve obtained at 80 °C for $Pt_{0.5}$–$Ru_{0.5}$ (BM)–Mg (dark squares). It shows that the dispersion technique had some success. Indeed, BET measurements indicate that the specific area of $Pt_{0.5}$–$Ru_{0.5}$ (BM)–Mg is 5.3 $m^2\ g^{-1}$ (for comparison, the specific area of all ball-milled and reference catalysts are summarized in Table 1). Because of the very high specific rate per catalytic site for $H_2$ oxidation [29], even a modest improvement in the specific area (and therefore of the number of available catalytic sites) of $Pt_{0.5}$–$Ru_{0.5}$ (BM)–Mg compared with $Pt_{0.5}$–$Ru_{0.5}$ (BM) is enough to drastically improve the performance of $Pt_{0.5}$–$Ru_{0.5}$ (BM)–Mg in pure $H_2$.

*Table 1.* Specific area of ball-milled and reference catalysts

| Catalyst | Specific area/$m^2\ g^{-1}$ |
|---|---|
| $Pt_{0.5}$–$Ru_{0.5}$ (BM) | 0.45 |
| $Pt_{0.5}$–$Ru_{0.5}$ (BM)–Mg | 5.3 |
| $Pt_{0.5}$–$Ru_{0.5}$ ($Mg_4$) | 23 |
| $Pt_{0.5}$–$Ru_{0.5}$ ($Al_4$) | 38 |
| Pt($Al_4$) | 21 |
| Pt Black | 44.3 |
| $PtRuO_x$ | 145 |
| $Pt_{0.5}$–$Ru_{0.5}$ Black | 63.2 |

However, when $H_2$ is substituted with $H_2$ + 100 ppm CO (Figure 4), the polarization curve of $Pt_{0.5}$–$Ru_{0.5}$ (BM)–Mg (dark squares) is the same as the polarization curve of Pt Black. The features of the polarization curve in the presence of CO has been interpreted by Springer et al. [29] on the basis of a simple kinetic model. These features include a low current density domain (here up to about 50 mA $cm^{-2}$) of good CO tolerance limited essentially by the maximum rate of hydrogen dissociative chemisorption on the small fraction of the catalyst surface area free of CO. Significantly higher voltage losses are incurred when attempting to exceed this typical limiting current density which is determined by the partial pressure of CO and the cell temperature. The availability of such uncovered sites for $H_2$ oxidation is related to the equilibrium coverage of the catalyst by CO at the relevant temperature and to any marginal catalytic activity of CO electrooxidation at low anode potential. It is stressed in the kinetic model that even very low CO electrooxidation currents may have a significant beneficial effect.

### 3.3. *$Pt_{0.5}$–$Ru_{0.5}$ ($Mg_4$) ball-milled catalysts*

It is possible to improve the availability of uncovered sites of the ball-milled catalysts by modifying the milling procedure. Instead of dispersing an already ball-milled $Pt_{0.5}$–$Ru_{0.5}$ (BM) by a second milling in Mg as described in the previous section, it is also possible to mill Pt, Ru, and Mg together and leach the resulting material in HCl after the milling step. This procedure is inspired from the Raney procedure used to improve the specific area of metals. It has already been used with mechanically alloyed metals [30]. In the present case, the Pt to Ru to Mg atomic ratio was chosen to be 1:1:8. The catalyst obtained after leaching Mg from the ball milled material is labelled $Pt_{0.5}$–$Ru_{0.5}$ ($Mg_4$).

The diffractogram of $Pt_{0.5}$–$Ru_{0.5}$ ($Mg_4$) is presented in Figure 5 (curve (a)). It consists of broad Pt peaks and sharper Ru peaks. There are no Mg peaks in the diffractogram after leaching the ball-milled material. The main Pt peak in $Pt_{0.5}$–$Ru_{0.5}$ ($Mg_4$) appears at the position expected for pure Pt (indicated by the vertical line). It implies that an eventual substitution of Pt by Ru or Mg in the Pt lattice is minimal. The fact that a $Pt_{0.5}$–$Ru_{0.5}$ alloy is not obtained when Pt is milled with Ru in the presence of Mg is probably due to the diluting effect of Mg whose atomic ratio far exceeds that of either Pt or Ru. On the other hand, the solubility of Mg in Pt has not been determined, while that of Pt in Mg is negligible [31].

From XRD data, it may be concluded that $Pt_{0.5}$–$Ru_{0.5}$ ($Mg_4$) is a composite material characterized by large Ru

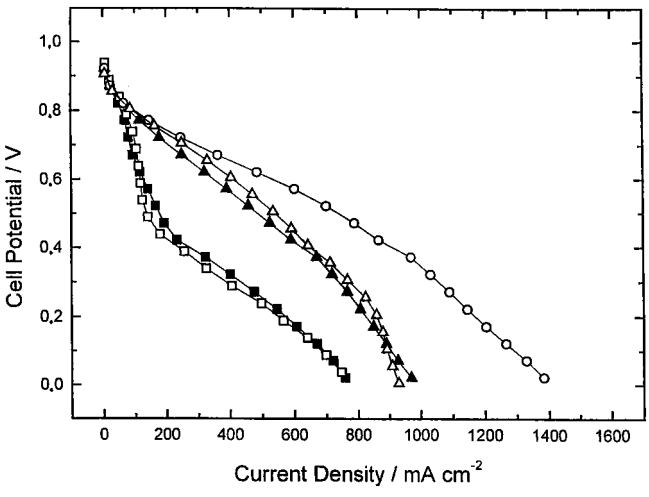


*Fig. 4.* $H_2$ + 100 ppm $CO/O_2$ polarization curves at 80 °C for a single membrane electrode assembly using (■) $Pt_{0.5}$–$Ru_{0.5}$ (BM)–Mg and (▲) $Pt_{0.5}$–$Ru_{0.5}$ ($Mg_4$) at the anode. Polarization curves with (□) Pt Black, (○) $Pt_{0.5}$–$Ru_{0.5}$ Black and (△) $PtRuO_x$ at the anode are given for comparison.

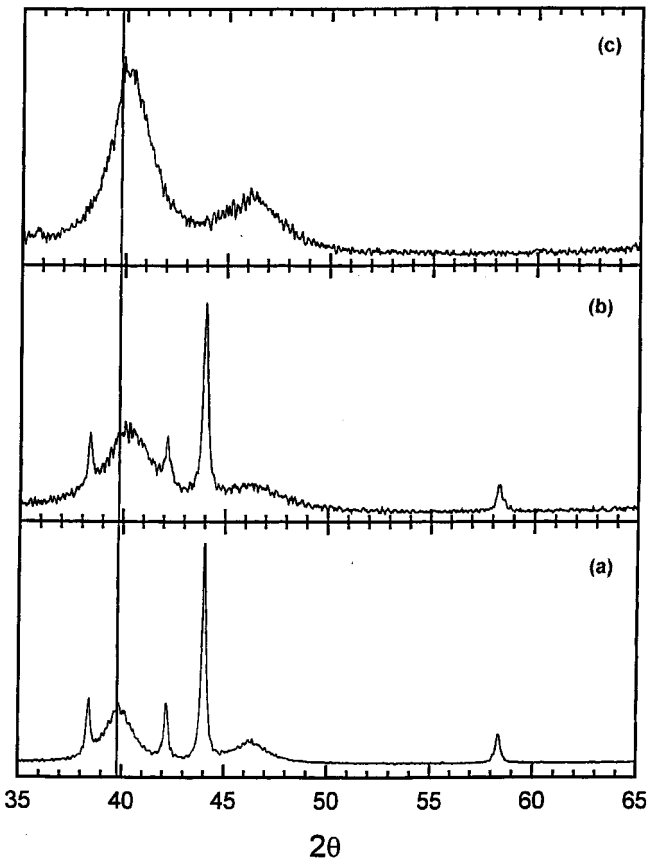


*Fig. 5.* X-ray diffractograms of: (a) $Pt_{0.5}$–$Ru_{0.5}$ ($Mg_4$), (b) $Pt_{0.5}$–$Ru_{0.5}$ ($Al_4$), (c) Pt ($Al_4$). Vertical line indicates the diffraction position of unalloyed Pt(1 1 1).

crystallites and smaller Pt crystallites that may contain some Ru but not enough to be able to have a definite influence on the lattice parameter of the Pt-Ru solid solution. The surface composition of $Pt_{0.5}$–$Ru_{0.5}$ ($Mg_4$) has been evaluated by XPS. The atomic ratio of Pt/Ru is 4.23 (equivalent to $Pt_{0.81}$–$Ru_{0.19}$). Considering the fact that 5.7 a/o Ru is soluble in liquid Mg at 800 °C [31], the solubility of Ru in Mg has to be considered. Thus the high Pt/Ru ratio found above may be explained by a loss of Ru into Mg that is subsequently leached, or by the fact that most of the Ru is too far from the surface of the larger Ru crystallites to participate in photoelectron generation. The Pt/O atomic ratio of the catalyst is 1.74.

The polarization curve obtained with $Pt_{0.5}$–$Ru_{0.5}$ ($Mg_4$) in pure $H_2$ at the anode is the same as that of $Pt_{0.5}$–$Ru_{0.5}$ (BM)–Mg already presented in Figure 3 (dark squares). The increase in active site density with the larger specific area (23 $m^2$ $g^{-1}$; Table 1) of $Pt_{0.5}$–$Ru_{0.5}$ ($Mg_4$) therefore has no influence on the rate of hydrogen oxidation. This rate was already at its maximum for the smaller number of available sites of $Pt_{0.5}$–$Ru_{0.5}$ (BM)–Mg, a lower specific area material (5.3 $m^2$ $g^{-1}$). On the other hand, the improvement in the specific area of $Pt_{0.5}$–$Ru_{0.5}$ ($Mg_4$) has a beneficial effect on the polarization curve obtained for that catalyst in $H_2$ + 100 ppm CO. This curve is shown in Figure 4 (filled triangles). The latter figure indicates that $Pt_{0.5}$–$Ru_{0.5}$ ($Mg_4$) and $PtRuO_x$ have comparable CO tolerance.

### 3.4. *$Pt_{0.5}$–$Ru_{0.5}$ ($Al_4$) and Pt ($Al_4$) ball-milled catalysts*

When the dispersion procedure used in the previous section is repeated with Al instead of Mg, another catalyst, $Pt_{0.5}$–$Ru_{0.5}$ ($Al_4$) is obtained after milling together Pt, Ru and Al in a 1:1:8 atomic ratio, respectively. In this case, Al is leached with 1 M NaOH. The polarization curve of $Pt_{0.5}$–$Ru_{0.5}$ ($Al_4$) in pure $H_2$ conditions at the anode is the same as that of $Pt_{0.5}$–$Ru_{0.5}$ (BM)–Mg presented in Figure 3 (dark squares), while Figure 6 shows the CO tolerance of the catalyst in $H_2$ + 100 ppm CO (dark circles). The latter figure indicates that $Pt_{0.5}$–$Ru_{0.5}$ ($Al_4$) and $Pt_{0.5}$–$Ru_{0.5}$ Black have comparable CO tolerance.

To determine the effect of Ru in $Pt_{0.5}$–$Ru_{0.5}$ ($Al_4$), a catalyst consisting of Pt ($Al_4$) was fabricated by ball-milling Pt and Al together in a 1 to 4 Pt/Al atomic ratio. In this case, Al was also leached in 1 M NaOH. The polarization curve of Pt($Al_4$) in pure $H_2$ at the anode is similar to that of $Pt_{0.5}$–$Ru_{0.5}$ (BM)–Mg presented in Figure 3 (filled squares), while Figure 6 shows the CO tolerance of the catalyst in $H_2$ + 100 ppm CO (filled diamonds). The latter figure indicates that even if Ru is

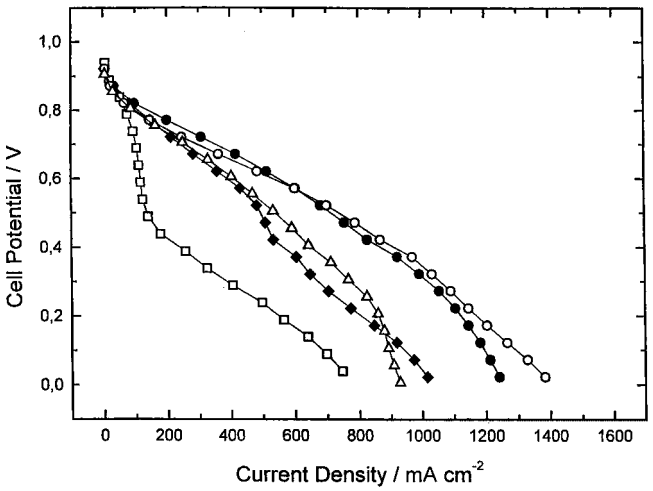


*Fig. 6.* $H_2$ + 100 ppm $CO/O_2$ polarization curves at 80 °C for a single membrane electrode assembly using (◆) Pt($Al_4$) and (●) $Pt_{0.5}$–$Ru_{0.5}$ ($Al_4$) at the anode. The polarization curves with (□) Pt Black, (○) $Pt_{0.5}$–$Ru_{0.5}$ Black and (△) $PtRuO_x$ at the anode are given for comparison.

absent from the composition of Pt($Al_4$), the catalyst nevertheless shows a better CO tolerance than that displayed by Pt Black (open squares in Figure 6). However, this CO tolerance slowly decreases under potentiostatic control at 0.5 V, as shown in Figure 7. These stability tests were run for 100 h except for $Pt_{0.5}$–$Ru_{0.5}$ ($Al_4$) for which the stability test was extended to 300 h. They also indicate that $Pt_{0.5}$–$Ru_{0.5}$ ($Al_4$) tested in the same conditions ($H_2$ + 100 ppm) than $Pt_{0.5}$–$Ru_{0.5}$ Black stabilizes at an even higher current density than the latter catalyst.

$Pt_{0.5}$–$Ru_{0.5}$ ($Al_4$) and Pt($Al_4$) were characterized in greater detail than the other catalysts. Their XRD

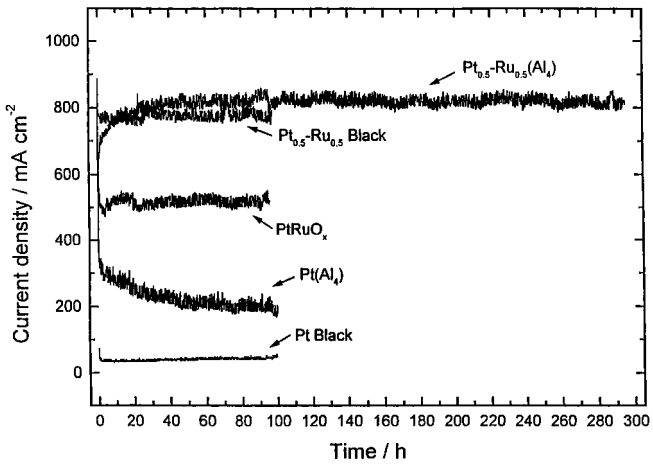


*Fig. 7.* Evolution at 0.5 V and 80 °C of the current density obtained for single membrane electrode assemblies using $Pt_{0.5}$–$Ru_{0.5}$ ($Al_4$), Pt($Al_4$), Pt Black, $Pt_{0.5}$–$Ru_{0.5}$ Black and $PtRuO_x$ as catalysts at the anode with 100 ppm CO in the $H_2$ feed.

diffractograms are given in Figure 5, curves (b) and (c), respectively. Except for the sharp Ru diffraction peaks in $Pt_{0.5}$–$Ru_{0.5}$ ($Al_4$), both diffractograms are similar. They both show broad Pt peaks shifted towards larger diffraction angles, indicating some dissolution of Al in the Pt lattice. The presence of an Al content in both $Pt_{0.5}$–$Ru_{0.5}$ ($Al_4$) and in Pt ($Al_4$) unleacheable in 1 M NaOH during the preparation of the catalyst is confirmed by neutron activation analysis revealing 1–3 wt % Al in the bulk of the materials. This confirms the existence of a Pt–Al solid solution which is expected for low Al content on the basis of the phase diagram for binary Pt–Al alloys [32]. On the other hand, based on: (i) the XRD diffractogram obtained for $Pt_{0.5}$–$Ru_{0.5}$ ($Mg_4$) (Figure 5(a)) where no shift of the Pt peaks was detected; and (ii) on the XRD diffractograms obtained for $Pt_{0.5}$–$Ru_{0.5}$ ($Al_4$) and $Pt_{0.5}$ ($Al_4$) (Figures 5(b) and (c) which show the same shift for Pt peaks, we believe that the Ru content of the Pt–Al solid solution is also low for $Pt_{0.5}$–$Ru_{0.5}$ ($Al_4$). Higher Ru contents might, however, be reacheable for longer milling times.

An average nanocrystallite size of 3.8 nm has been evaluated from the width at half height of the main diffraction peak (Pt(1 1 1)) of Pt($Al_4$) in Fig. 5(c). Since the same peak shows a similar broadness for $Pt_{0.5}$–$Ru_{0.5}$ ($Al_4$), a similar nanocrystallite size is also expected for that catalyst. The specific area measured for $Pt_{0.5}$($Al_4$) is 21 $m^2\ g^{-1}$ and it is 38 $m^2\ g^{-1}$ for $Pt_{0.5}$–$Ru_{0.5}$ ($Al_4$). These relatively large specific areas for ball-milled materials explain why these catalysts perform well in the oxidation of pure $H_2$. It remains to explain why they are also CO tolerant.

The surface species of $Pt_{0.5}$–$Ru_{0.5}$ ($Al_4$) have been evaluated by XPS. Figure 8 presents the XPS spectra at the Pt 4f core level of $Pt_{0.5}$–$Ru_{0.5}$ ($Al_4$) (curve (c)) and of the three references: Pt Black (curve (a)), $Pt_{0.5}$–$Ru_{0.5}$ Black (curve (b)) and $PtRuO_x$ (curve (d)). The XPS spectrum at the Pt 4f core level of $Pt_{0.5}$ ($Al_4$) has already been presented [33]. It is the same as that of Pt Black. The vertical lines at 71.0, 72.4 and 73.8 eV are the binding energies reported for the $4f_{7/2}$ peak of Pt [34], $Pt(OH)_2$ [34] and PtO [35], respectively. From Figure 8, it may be deduced that $PtRuO_x$ (curve (d)) contains a large amount of oxidized Pt. A small amount of oxidized Pt is also detected on $Pt_{0.5}$–$Ru_{0.5}$ Black (curve (b)), while both Pt Black (curve (a)) and $Pt_{0.5}$–$Ru_{0.5}$ ($Al_4$) show similar XPS spectra characteristic of metallic Pt.

Figure 9 presents XPS spectra at the Ru 3d core level of $Pt_{0.5}$–$Ru_{0.5}$ ($Al_4$) (curve (b)) and the two references containing Ru: $Pt_{0.5}$–$Ru_{0.5}$ Black (curve (a)) and $PtRuO_x$ (curve (c)). The vertical lines at 280.0 and 280.7 eV are the binding energies reported for the $3d_{5/2}$peaks of Ru and $RuO_2$, respectively [36]. From Figure 9, it may be

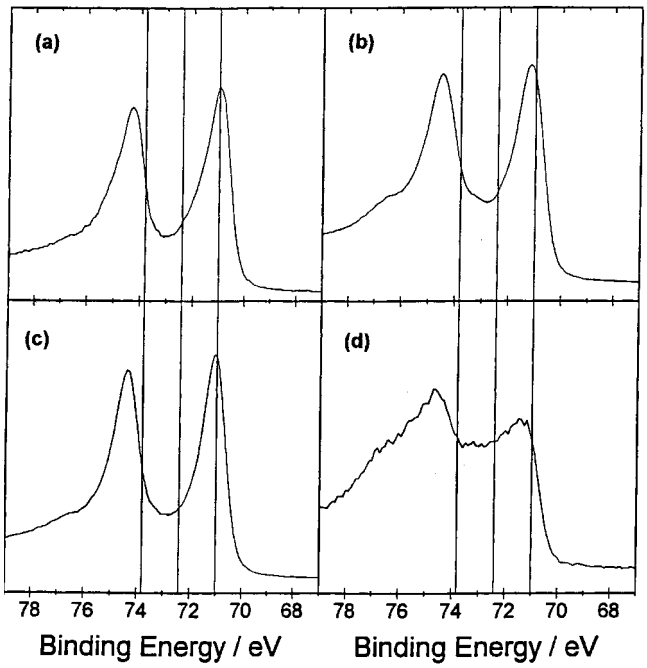


*Fig. 8.* XPS spectra at the Pt 4f core levels of (a) Pt Black; (b) $Pt_{0.5}$–$Ru_{0.5}$ Black; (c) $Pt_{0.5}$–$Ru_{0.5}$ ($Al_4$); and (d) $PtRuO_x$. The vertical lines at 71.0, 72.4 and 73.8 eV are the binding energies reported for the $4f_{7/2}$ peaks of Pt, $Pt(OH)_2$ and PtO, respectively.

deduced that $PtRuO_x$ contains oxidized ruthenium exclusively, while $Pt_{0.5}$–$Ru_{0.5}$ Black and $Pt_{0.5}$–$Ru_{0.5}$ ($Al_4$) contain both metallic and oxidized Ru.

To obtain the oxidation state for Al on the surface, it was necessary to measure the Al 2s XPS spectrum. Al 2p, which is the principal peak of Al, was not accessible since its binding energy coincides with that of Pt (72.65 eV for metallic Al [37]). Furthermore, its sensitivity factor is only 0.537 against 15.46 for Pt. It was therefore not possible to determine the presence of Al at the surface of the catalyst from the Al 2p peak. The Al 2s core level of $Pt_{0.5}$–$Ru_{0.5}$ ($Al_4$) (curve (a)) is given in Figure 10 Curves (b) and (c) are the Al 2s core level spectra of an Al sheet before and after etching to remove the upper oxidized layer. The vertical lines in Figure 10 indicate the binding energy of metallic Al (117.8 eV), $Al_2O_3$(119.6 eV), and oxidized metallic Al (120.5 eV). Curve (a) indicates that metallic Al and oxidized Al are therefore present at the probed surface of $Pt_{0.5}$–$Ru_{0.5}$ ($Al_4$).

The surface compositions of $Pt_{0.5}$–$Ru_{0.5}$ ($Al_4$) and Pt ($Al_4$) have been estimated by XPS. For $Pt_{0.5}$–$Ru_{0.5}$ ($Al_4$), the atomic ratio Pt/Ru is 1.23 (equivalent to $Pt_{0.55}$–$Ru_{0.45}$) while the atomic ratio of Pt/O is 0.29. For Pt($Al_4$), the atomic ratio of Pt/O is 0.53. The characterization of $Pt_{0.5}$–$Ru_{0.5}$ ($Al_4$) indicates that this catalyst is

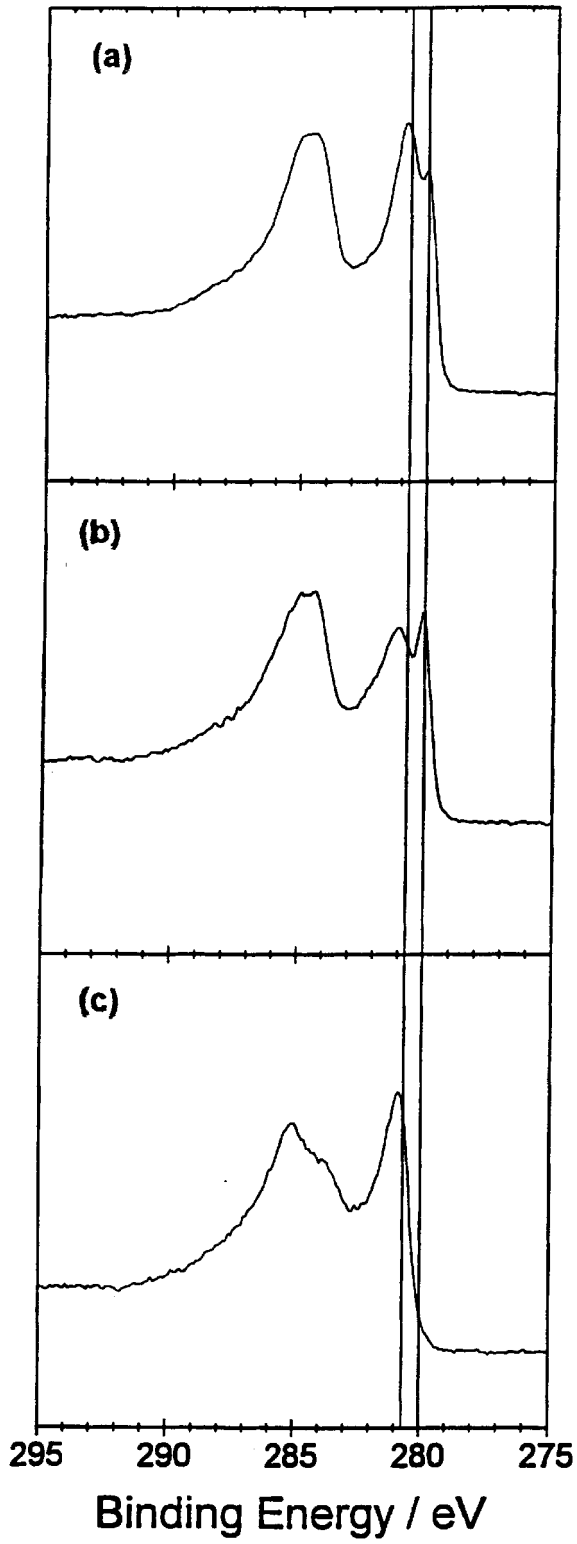


*Fig. 9.* XPS spectra at the Ru 3d core levels of (a) $Pt_{0.5}$–$Ru_{0.5}$ Black; (b) $Pt_{0.5}$–$Ru_{0.5}$ ($Al_4$); and (c) $PtRuO_x$. The vertical lines at 280.0 and 280.7 eV are the binding energies reported for the $3d_{5/2}$ peak of Ru and $RuO_2$, respectively.

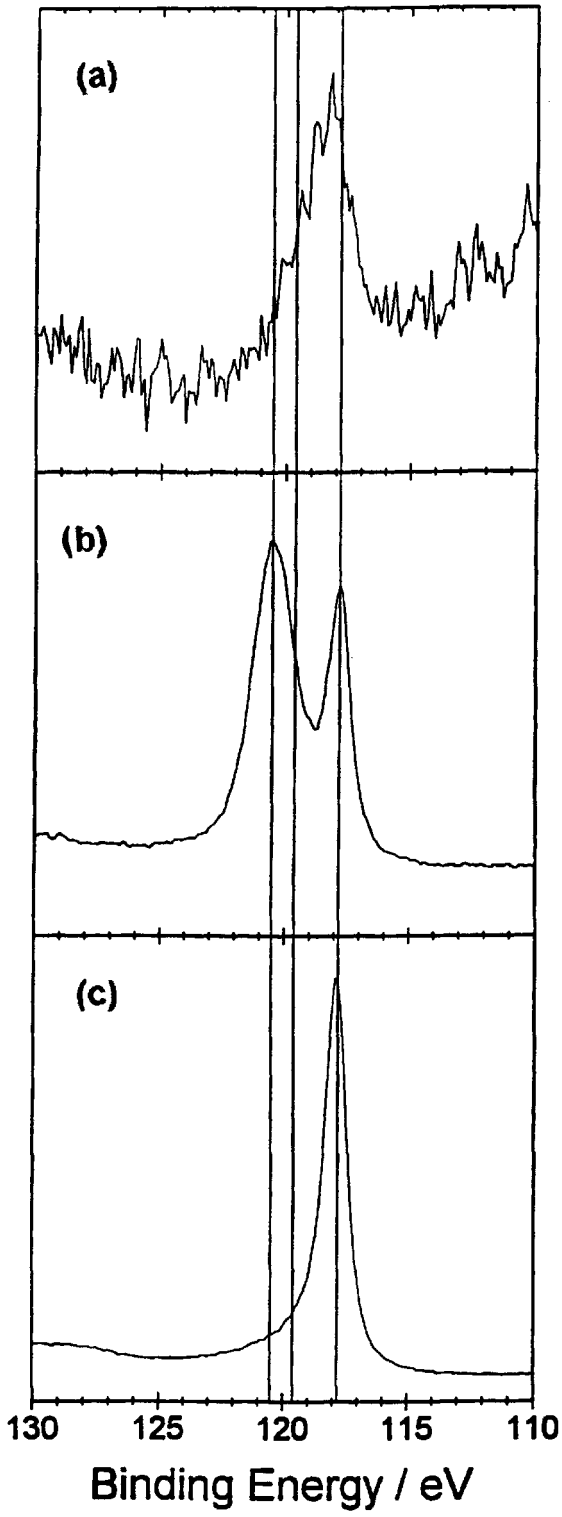


*Fig. 10.* XPS spectra at the Al 2s core level of (a) $Pt_{0.5}$–$Ru_{0.5}$ ($Al_4$); (b) an Al film with its native oxidation layer and (c) an Al film after etching the oxidation layer. The vertical lines at 117.8, 119.6 and 120.5 eV are the binding energies for the Al 2s of Al, $Al_2O_3$, and oxidized metallic Al, respectively.

a composite of low Ru content small Pt–Al alloy crystallites in contact with larger Ru nanocrystals. In the Pt-Al (+Ru) alloy crystallites, Pt is exclusively metallic while Al is partially oxidized. However, larger Ru crystallites are also partially oxidized. This catalyst is as CO tolerant as $Pt_{0.5}$–$Ru_{0.5}$ Black. Its composite structure ressembles that of $Pt/WO_3$ and $Pt–Ru/WO_3$, two CO tolerant catalysts of composite structure, which have also been tested as catalysts for the direct oxidation of methanol [38, 39].

Since the Al content of $Pt_{0.5}$–$Ru_{0.5}$ ($Al_4$) is 1 to 3 wt %, it is possible that this Al may leach into the membrane in fuel cell conditions. The stable current output measured over 300 h (Figure 7) already indicates that if there is Al leaching, it should be minimal. Quantitative results were obtained by neutron activation analysis (accuracy on the measurements: ±5%). After completion of the test, electrodes were peeled off the membrane–electrode assembly and the Al content in the membrane was measured. An amount of 241 ppm Al was detected in that membrane while the Al content of a virgin membrane was 2.1 ppm. On the other hand, 6022 ppm of Al were measured in a membrane left for 40 h at 25 °C in a saturated aqueous solution of $AlNH_4(SO_4)_2$. In that case, $NH_4^+$ and $Al^{3+}$ replaced the protons in the membrane. A value of 6080 ppm Al in the membrane is calculated on the basis of 0.91 $H^+$equivalent per kg of Nafion 117® [40] for the membrane in contact with $AlNH_4(SO_4)_2$; this theoretical Al content agrees well with the Al content found experimentally. The saturation level of Al in a Nafion® membrane is then calculated to be 8140 ppm. Therefore, an Al content of 241 ppm measured after a 300 h test in fuel cell represents only 3% of the Al saturation level in the membrane. This is very little taking into account the fact that the Al content of $Pt_{0.5}$–$Ru_{0.5}$ ($Al_4$) is 1–3 wt %. Indeed, if all the Al in the catalyst was leaching into the membrane, it would represent between 1.3 to 4 times its saturation level (8140 ppm).

## 4. Conclusions

It has been shown that it is possible to obtain, by high energy ball milling, an unsupported catalyst composed of Pt, Ru and Al displaying a CO tolerance similar to that of the best commercial unsupported Pt–Ru catalysts characterized by the same Pt/Ru atomic ratio of 1. This catalyst shows stable behaviour under $H_2$ + 100 ppm CO (at least for 300 h).

It has also been shown that a simple milling of Pt and Ru to form an alloy of the type $Pt_{0.5}$–$Ru_{0.5}$ (BM) is not enough to obtain a performing catalyst, even if nanocrystals of the alloy are obtained by ball milling. Nanocrystals have a tendency to aggregate during the milling step, drastically reducing the specific area of the materials. In order to obtain catalytic performances for the oxidation of $H_2$ equivalent to those of commercial catalysts, it is necessary to increase the specific area of the ball-milled materials to at least 5 $m^2\ g^{-1}$. However, this is not enough for the oxidation of $H_2$ in the presence of 100 ppm CO. The best dispersion of the ball-milled nanocrystals is obtained by a Raney type process using a leacheable metal like Al or Mg, which is ball-milled with Pt and Ru. The most performing catalyst is obtained when the leacheable metal is Al. This catalyst has been labelled $Pt_{0.5}$–$Ru_{0.5}$ ($Al_4$). This catalyst has a specific area of 38 $m^2\ g^{-1}$, which is the highest area measured among all ball-milled catalysts studied in this work. It is, however, still lower than the specific area of all the unsupported catalysts used as references in this study. $Pt_{0.5}$–$Ru_{0.5}$ ($Al_4$) is a composite catalyst containing nanometric crystallites (~4 nm) of a Pt–Al alloy with a low Ru content and larger Ru crystallites which are partially oxidized. The Al content in the catalyst is of the order of 1–3 wt %. XPS results show that metallic and oxidized aluminum are present at the surface of the catalyst. Stability experiments of membrane electrode assemblies and the dosimetry of Al in the membrane demonstrate however that very little Al is found in the membrane after 300 h of fuel cell operation.

Now that the use of BM in CO tolerant Pt-based catalysts has been established, the production by the same industrially amenable technique of Pt-based catalysts other than $Pt_{0.5}$–$Ru_{0.5}$ ($Al_4$) may be contemplated.

## Acknowledgements

This work was supported by Hydro-Québec and a Collaborative R&D grant from NSERC.

## References

1. K.B. Prater, *J. Power Sources* **61** (1996) 105.
2. A.J. Appleby, *Phil. Trans. R. Soc. Lond.* **A354** (1996) 1681.
3. G.J.K. Acres and G.A. Hards, *Phil. Trans. R. Soc. Lond.* **A354** (1996) 1671.
4. S. Gottesfeld and T.A. Zawodzinski, *Adv. Electrochem. Sci. Eng.* **5** (1997) 195.
5. A.J. Appleby and F.R. Foulkes, *Fuel Cell Handbook*, Krieger Publishing Company, Malabar, FA.
6. N.E. Vanderborgh, J. Guante, R.E. Dean and R.D. Sutton, Abstract of the Fuel Cell Seminar in Long-Beach, CA. (Oct. 1988), Courtesy Associates, Inc., Washington, DC, p. 52.
7. S. Gottesfeld and J. Pafford, *J. Electrochem. Soc.* **135** (1988) 2651.

8. D. Wilkinson and D. Thompsett, Proceedings of the Second International Symposium on *New Materials for Fuel Cell and Modern Battery Systems*, O. Savadogo and P. R. Roberge (eds), Ecole Polytechnique Montreal, 1997, p. 266.
9. S. Wasmus and W. Vielstich, *J. Appl. Electrochem.* **23** (1993) 120.
10. B. Bittins-Cattaneo, S. Wasmus, B. Lopez-Mishima and W. Vielstich, *J. Appl. Electrochem.* **23** (1993) 625.
11. H.A. Gasteiger, N. Markovic, P.N. Ross, Jr and E.J. Cairns, *J. Phys. Chem.* **98** (1994) 617.
12. P.N. Ross, K. Kinoshita, A.J. Scarpellino and P. Stonehart, *J. Electroanal. Chem.* **63** (1975) 97.
13. V.B. Hughes and R. Miles, *J. Electroanal. Chem.* **145** (1983) 87.
14. M. Watanabe and S. Motoo, *J. Electroanal. Chem.* **60** (1975) 267.
15. H.A. Gasteiger, N.M. Markovic and P. N. Ross, Jr, *J. Phys. Chem.* **98** (1994) 8290.
16. H.A. Gasteiger, N.M. Markovic and P.N. Ross, Jr, *J. Phys. Chem.* **99** (1995) 8945.
17. X. Ren, M.S. Wilson and S. Gottesfeld, In: S. Gottesfeld, G. Halpert and A. Landgrebe (eds) *Proton Conducting Membrane Fuel Cells I*, The Electrochemical Society, Pennington, NJ, 1995, p. 252.
18. E. Reddington, A. Sapienza, B. Gurau, R. Viswanathan, S. Sarangapani, E.S. Smotkin and T.E. Mallouk, *Science* **280** (1988) 1735.
19. M.P. Hogarth and G.A. Hards, *Platinum Metals Rev.* **40** (1996) 150.
20. C.C. Koch, In: R.W. Cahn (ed.) *Materials Science and Technology, Vol 15, Processing of Metals and Alloys*, VCH, Verlagsgesellschaft, Weinheim, (1991), chapter 5, p. 193.
21. H. Gleiter, *J. Appl. Crystallography*, **24** (1991) 79.
22. A.W. Weber and H. Bakker, *Physica B* **153** (1988) 93.
23. R.B. Schwarz and C.C. Koch, *Appl. Phys. Lett.* **49** (1986) 146.
24. T. Masumoto, K. Hashimoto and M. Naka, In: B. Cantor (ed.) Proceedings of the the 3rd International Conference on *Rapidly Quenched Metals*, vol. 2, B., The Metal Society, London, (1978) p. 435.
25. R.M. Davis, B. McDermott and C.C. Koch, *Metall. Trans. A* **19A** (1988) 2867.
26. J.M. Hutchinson, *Plat. Met. Rev.* **16** (1972) 88.
27. B.E. Warren, *X-ray Diffraction*, Dover Publication, New York.
28. J. Huot, S. Bouaricha, S. Boily, J.P. Dodelet, D. Guay and R. Schulz, *J. Alloys & Compounds* **266** (1998) 307.
29. T. Springer, T. Zawodzinski and S. Gottesfeld, In: J. McBreen, S. Mukerjee and S. Srinivasan (eds) Proceedings of the symposium on *Electrode Materials and Processes for Energy Conversion and Storage IV*, The Electrochemical Society, Pennington, NJ, **97-13** (1997) p. 15.
30. E. Ivanov, S.A. Makhlouf, K. Sumiyama, H. Yamauchi, K. Suzuki and G. Golubkuva, *J. Alloys and Compounds* **185** (1992) 25.
31. A.A. Nayeb-Hashemi and J.B. Clark, Eds, *Phase Diagrams of Binary Magnesium Alloys*, ASM International, Metals Park, OH (1988) p. 257.
32. T.B. Massalski (Ed.), *Binary Alloy Phase Diagram*, 2nd edn., ASM International Materials Park, OH.
33. M.C. Denis, G. Lalande, D. Guay, J.P. Dodelet and R. Schulz, In: J. McBreen, S. Mukerjee and S. Srinivasan (eds), Proceedings of the symposium on *Electrode Materials and Processes for Energy Conversion and Storage IV*, The Electrochemical Society, Pennington, NJ, **97-13** (1997) p. 119.
34. J.S. Hammond and N. Winograd, *J. Electroanal. Chem.* **78** (1977) 55.
35. J.B. Goodenough, A. Hamnett, B.J. Kennedy, R. Manoharan and S.A. Weeks, *J. Electroanal. Chem.* **240** (1988) 133.
36. K.S. Kim and N. Winograd, *J. Catal.* **35** (1974) 66.
37. C.D. Wagner, W.W. Riggs, L.E. Davis, J.F. Moulder and G.E. Muilenberg, *Handbook of X-ray Photoelectron Spectroscopy*, Perkin–Elmer Corporation. 1978.
38. P.K. Shen and A.C.C. Tseung, *J. Electrochem. Soc.* **141** (1994) 3082.
39. P.K. Shen, K.Y. Chen and A.C.C. Tseung, *J. Electrochem. Soc.* **142** (1995) L85.
40. T. A. Zawodzinski, T. E. Springer, F. Uribe and S. Gottesfeld, *Solid State Ionics* **60** (1993) 199.